Derivation of Operation Mode for Flying Capacitor Topology Applied to Three-level DAB converter

Hayato Higa and Jun-ichi Itoh
Department of Electrical Engineering
Nagaoka University of Technology
Niigata, Japan
hhiga@stn.nagaokaut.ac.jp, itoh@vos.nagaokaut.ac.jp

Abstract— **This paper discusses a Dual Active Bridge (DAB) DC-DC converter utilizing to three-level flying capacitor topology for a battery conversion system. With applying to a multi-level topology, the voltage stress is reduced in all switches. In addition, the low order harmonic components are reduced due to five-level waveform. In a two-level DAB converter, the efficiency becomes low when the input voltage is not closed to the nominal voltage. In order to improve the efficiency at the input voltage fluctuation, this paper also proposes the operation mode of the three-level DAB converter at the input voltage fluctuation. The output voltage waveform of the inverter is determined by the relationship among the efficiency of the two modes which are so called the full-bridge mode and the half-bridge mode. In this paper, the changing point between the half-bridge and the full-bridge mode is derived using the loss calculation. In the simulation, the ZVS range and the inductor current are compared with the two-level and the three-level inverter. It is confirmed that the ZVS range is extended by 60%. In addition, the fundamental operation of the proposed DAB converter is confirmed by the experimental results.**

I. INTRODUCTION

Recently, energy storage systems have attracted for electric vehicles and smart grid systems. A bi-directional isolated DC-DC converter is used as the battery interface system. A dual active bridge (DAB) converter has been studied actively as a bi-directional isolated DC-DC converter [1-3]. The DAB converter obtains the high efficiency and the high power density because zero voltage switching (ZVS) is achieved during the dead-time using an additional capacitor or a parasitic capacitance of the switching devices [4]. However, the ZVS range of the DAB converter is limited by the error between the ratio of the input/output voltage and the transformer turn ratio [5]. Furthermore, reactive current is also increased at light load for the same reason. When the ratio of the input /output voltage fluctuates in the system, the efficiency of the DAB converter decreases at light load. In order to solve these problems, Pulse Width Modulation (PWM) is added to the phase shift control in order to extend the ZVS range and reduce the circulating current in [6-7]. However, it is not always possible to achieve the ZVS for all switches due to the error between the input/output voltages including the turn ratio of the transformer.

On the other hand, the multi-level DAB converter in which a multi-level inverter is applied to the high voltage side has been proposed. The multi-level inverter can reduce the voltage stress of switching devices [8]. In [9], a three-level DAB converter with a neutral-point-clamped topology has been proposed in order to improve the total harmonic distortion of the inductor current. However, ZVS is not achieved because the drain-to-source voltage is clamped by clamped diode during dead-time period. Moreover, the voltage balance control is required. On the other hand, a three-level DAB converter applied with T-type topology has been proposed in order to achieve the minimum inductor current [10]. The switching pattern of the three-level inverter is determined by the relationship among the turn ratio of the transformer and the input/output voltage. However, this literature has not discussed the ZVS operation though the voltage stress of the bidirectional switch is reduced by the T-type three-level inverter.

This paper proposes the three-level DAB converter applied with a flying capacitor topology. With the three-level flying capacitor topology, the voltage stress is reduced in all switches in the high voltage side. The switching patterns are determined by the loss calculation. This paper is organized as follows; first, the circuit configuration of the three-level DAB converters is introduced. Second, the operation mode of the three-level DAB converter is explained. Thirdly, the operation mode of the three-level DAB converter is determined by the loss calculation results. Fourth, the three-level DAB converter and the two-level DAB converter are demonstrated from the

simulation. From the simulation results, the ZVS range and the inductor current are compared with the three-level DAB converter and the conventional two-level DAB converter. Finally, the fundamental operation is confirmed by the prototype of the proposed DAB converter.

II. PROPOSED CIRCUIT

Fig. 1 shows the configuration of the two-level DAB converter. This converter consists of the high frequency transformer and the two voltage source inverters with H-bridge topology. If the voltage fluctuation occurs. The ZVS range is limited and the circulating current is increased.

Fig. 2 shows the configuration of the three-level DAB converter with a flying capacitor topology. The three-level DAB converter comprises a flying capacitor three-level inverter at the primary side of the transformer and a two-level inverter at the secondary side of the transformer. It should be noted that the three-level inverter is applied to the high voltage side. Thus, the voltage stress of the switching devices is reduced compared to two-level inverter. Therefore, a high performance MOSFET can be used.

Fig. 3 shows the switching pattern of the three-level DAB converter when the output voltage of the three-level inverter is the five-level waveform (five-level mode). In Fig. 2, the each voltage level period is determined by the half voltage period of arm voltage α and the phase difference between each arm voltage β. In addition, the output voltage of the three-level inverter is square waveform which has the voltage level; $\pm V_{in}$ (Full-bridge mode) when α, β are zero. Similarly, the output voltage of the three-level inverter is the square voltage waveform which has voltage levels; $\pm 1/2\,V_{in}$ (Half-bridge mode) when the half voltage period of the arm voltage α is zero and the phase difference between each arm voltage β is $\pi/2$ rad. (1)

A. Output power of full-bridge mode and half-bridge mode

When the primary side of the transformer is operated as the full-bridge converter, the output power to the secondary side P_{out_FB} is expressed by (1) [1]

$$P_{out\_FB} = \frac{V_{in}V_{out}}{N\omega L}\left(\delta - \frac{\delta^2}{\pi}\right) \quad \text{..... (1)}$$

Where ω is switching angular frequency, N is a turn ratio of the high frequency transformer. δ is a phase difference between the primary side voltage and the secondary side voltage of the transformer.

When the secondary side of the transformer is operated as the half-bridge converter, the amplitude of the secondary voltage of the transformer becomes $V_{in}/2$. In the half-bridge mode, the output power to the secondary side P_{out_HB} is expressed by (2).

$$P_{out\_HB} = \frac{V_{in}V_{out}}{2N\omega L}\left(\delta - \frac{\delta^2}{\pi}\right) \quad \text{..... (2)}$$

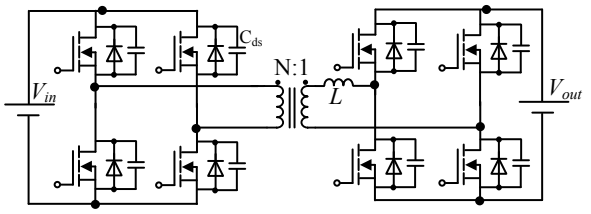

Fig. 1. Configuration of two-level DAB converter. The primary side (high voltage side) and the secondary side (low voltage side) is applied with the two-level inverter.

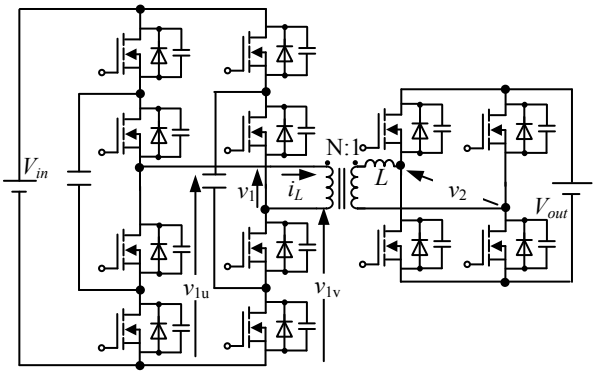

Fig. 2. Configuration of three-level DAB converter. The primary side (high voltage side) is applied with flying capacitor three-level inverter. the secondary side (low voltage side) is applied with the two-level inverter.

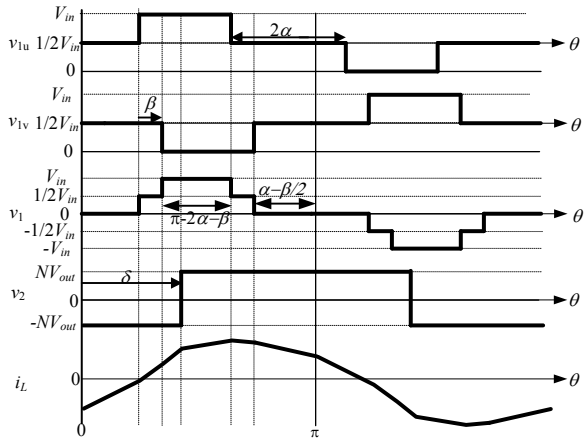

Fig. 3. Switching pattern of three-level DAB converter. The each voltage level is determined by the half of the input voltage level period α and the phase difference of the each arm voltage β.

From (2), the output power at the full-bridge mode is smaller than the output power at the half-bridge mode.

B. Inductor current of full-bridge mode and half-bridge mode

The inductor current of the full-bridge mode I_{L_FB} against the phase difference δ is obtained by (3) [1].

$$I_{L\_FB} = \frac{\sqrt{V_{in}V_{out}}}{N\omega L}\sqrt{-\frac{4}{3\pi}\delta^3 + \delta^2 + \frac{\pi^2}{12}\frac{N(V_{in} - NV_{out})^2}{V_{in}V_{out}}} \quad \text{..... (3)}$$

From (3), the inductor current is increased by the error between the turn ratio of the transformer N and the output/primary

voltage V_{out}/V_{in}. On the other hands, the inductor current of the half-bridge mode I_{L_HB} is obtained by (4).

$$I_{L\_HB} = \frac{\sqrt{V_{in}V_{out}}}{\sqrt{2}N\omega L}\sqrt{-\frac{4}{3\pi}\delta^3 + \delta^2 + \frac{\pi^2}{6}\frac{N(V_{in}/2 - NV_{out})^2}{V_{in}V_{out}}} \quad \text{..... (4)}$$

From (4), the inductor current is minimum when the value of NV_{out}/V_{in} is close to 0.5.

C. ZVS range of full-bridge mode and half-bridge mode

In order to achieve ZVS for all switching devices, the condition of the output power is presented by (5)[5].

$$\frac{V_{in}V_{out}}{N\omega L}\frac{\pi}{4}\left\{\left|1-\left(\frac{NV_{out}}{V_{in}}\right)^2\right|\right\} \le P_{out\_FB} \le \frac{V_{in}V_{out}}{N\omega L}\frac{\pi}{4} \quad \text{..... (5)}$$

In general, the operation range of the DAB converter is $-\pi/2 < \delta < \pi/2$. Hence, the right side of (5) is the rated power. From (5), the lower limit of the output power to achieve the ZVS increases due to the ratio of the primary and the secondary voltage including the turn ratio of the transformer NV_{out}/V_{in} .

On the other hands, the condition of the output power is presented by (6) in order to achieve the ZVS in the half-bridge mode.

$$\frac{V_{in}V_{out}}{N\omega L}\frac{\pi}{4}\left\{\left|1-4\left(\frac{NV_{out}}{V_{in}}\right)^2\right|\right\} \le P_{out\_HB} \le \frac{V_{in}V_{out}}{N\omega L}\frac{\pi}{8} \quad \text{..... (6)}$$

From (6), The ZVS range at the half-bridge mode is wider than the full-bridge mode at light load when NV_{out}/V_{in} is close to 0.5. At the half-bridge mode, the ZVS is achieved at light load compared to full-bridge mode. On the othrer hand, the ZVS is achieved at a heavy load at the full-bridge mode. As a result, the ZVS range is extended due to changing operation between half-bridge mode and full-bridge mode.

In the proposed circuit, the efficiency can be improved for wide load variation by designing the ZVS range and adjusting the ratio among the conduction loss, the copper loss and the iron loss of the transformer. Therefore, it is necessary to calculate the each loss in order to derive the changing point the operation mode.

III. DERIVATION OF OPERATION MODE FROM LOSS CALCULATION

This section explains the power loss expression of the proposed circuit. The switching loss is ideally zero, because the switching devices can achieve the ZVS. The power loss of the proposed circuit consists of the conduction loss and the constant loss. The conduction loss is generated in the on-resistance of MOSFET, the wire resistance of the transformer. The constant loss is generated within the iron loss of the transformer and the no load loss.

A. Mathmatical loss expression

The power loss of the MOSFET consists of the conduction loss. In the secondary voltage side inverter of Fig. 1, the conduction loss of the secondary voltage side MOSFET $P_{condloss\_pr}$ can be obtained by (7) using the on-resistance of the secondary side MOSFET R_{on_pr}. Thus, the power loss per secondary MOSFET $P_{condloss\_se}$ can be obtained by (8) using the on-resistance of the secondary side MOSFET

$$P_{condloss\_pr} = 4R_{on\_pr}(I_L/2)^2 \quad \text{..... (7)}$$

$$P_{condloss\_se} = 2R_{on\_se}(NI_L/2)^2 \quad \text{... (8)}$$

In the half-bridge mode, the inductor current is double compared to the full-bridge mode at same load.

The power loss of the transformer consists of the iron loss and the copper loss. The iron loss occurs because of the flux change in the core. The copper loss occurs in the winding resistance of transformer. At first, when the square wave is input to the transformer, the flux density ΔB is obtained by (9).

$$\Delta B = \frac{V_1 \cdot t_{on}}{2N_1 A_c} \quad \text{..... (9)}$$

where V_1 is the input voltage of the transformer, N_2 is the secondary wire turns, A_c[m^2] is the effective cross-section of the core. Therefore, the iron loss of the transformer P_{trans_fe} is obtained by (10) using the characteristics of the flux density - core loss value P_{cv}[W/m^3] and the effective volume of the core V_e[m^3]. In the half-bridge mode, the iron loss is decreased by decrement of the flux density.

$$P_{trans\_fe} = P_{cv}V_e \quad \text{..... (10)}$$

The copper loss of the transformer is obtained from the winding resistance with the skin effect. The primary winding copper loss P_{copper_pr} in the main circuit is obtained by (11) using the primary winding resistance of the main circuit with skin effect R_{wire_pr}. The secondary winding copper loss P_{copper_se} in the main circuit is obtained by (12) using the primary winding resistance of the main circuit with skin effect R_{wire_se}.

$$P_{copper\_pr} = R_{wire\_pr}I_L^2 \quad \text{..... (11)}$$

$$P_{copper\_se} = R_{wire\_se}(NI_L)^2 \quad \text{..... (12)}$$

The power loss of the additional inductor consists of the copper loss and the iron loss. In order to neglect the saturation of the flux in the core, the air coil is used. Thus, the copper loss occurs only in the additional inductor. The copper loss of the additional inductor is obtained by similarly to (9).

The root mean square value of the inductor current is charged or discharged to the output and the input capacitor. Therefore, the output capacitor loss $P_{loss\_C\_out}$, $P_{loss\_C\_in}$ are obtained by (13), (14) using the equivalent series resistance R_{C_out}, R_{C_in}.

$$P_{loss\_C\_in} = R_{C\_in}I_L^2 \quad \text{..... (13)}$$

$$P_{loss\_C\_out} = R_{C\_out}NI_L^2 \quad \text{..... (14)}$$

B. Derivation of changing point

At the changing point, the loss of the full bride mode is equal to the half-bride mode. The relationship between the loss and the inductor current is is presented by (15).

$$(I_{L\_HB}{}^2 - I_{L\_FB}{}^2) = \frac{P_{trans\_fe\_FB} - P_{trans\_fe\_HB}}{\{N^2 R_{se} + R_{pr}\}} \quad \text{..... (15)}$$

where $P_{trans\_fe\_FB}$ is the iron loss at the full-bridge mode, $P_{trans\_fe\_HB}$ is the iron loss at the half-bridge mode, R_{pr} is the sum of the on-resistance of the primary side MOS-FETs, equivalent series resistance of the input capacitance, the primary side wire resistance of the transformer, R_{se} is the sum of the secondary side resistance. In order to derive the output power of the changing point, the derivation of the phase difference is needed from (1) or (2). At the changing point, the phase difference of the half-bridge mode is about the half of the phase difference the full-bridge mode. Therefore, it is possible to derive the changing point using the only phase difference of the full-bridge mode. On the other hand, the each mode of the inductor current is varied by NV_{out}/V_{in} from (3). Therefore, the phase difference at the changing point is derived using the two conditions according to NV_{out}/V_{in}. At the first condition of $0.75 \geq NV_{out}/V_{in}$, the equation (4) is approximated. The phase difference at the changing point $\delta_{HB\text{-}FB}$ is presented by (16) at the first condition using (15), (3) of approximation and (4).

$$\delta_{\_HB-FB} = \frac{\pi}{5}\left\{\frac{7}{4}\frac{(N\omega L)^2}{V_{in}V_{out}}\frac{P_{trans\_fe\_FB} - P_{trans\_fe\_HB}}{(N^2 R_{se} + R_{pr})} - \frac{13}{10}\frac{(V_{in}/2 - NV_{out})^2}{NV_{in}V_{out}} + \frac{2}{5}\right\}$$

....(16)

At the second condition of $1 \geq NV_{out}/V_{in} > 0.75$, the equation (3) is approximated. Therefore, the phase difference at the changing point $\delta_{HB\text{-}FB}$ is presented by (17) using (15), (4) of approximation and (3).

$$\delta_{\_HB-FB} = \frac{\pi}{5}\left\{\frac{7}{4}\frac{(N\omega L)^2}{V_{in}V_{out}}\frac{P_{trans\_fe\_FB} - P_{trans\_fe\_HB}}{(N^2 R_{se} + R_{pr})} + \frac{13}{10}\frac{(V_{in} - NV_{out})^2}{NV_{in}V_{out}} + \frac{2}{5}\right\}$$

....(17)

The output power at the changing point is derived by (16) or (17), (1).

IV. LOSS CALCULATION RESULTS

Fig. 4 shows the loss calculation results against the output power at the fluctuation of the primary and the secondary voltage. From the results, the maximum efficiency of over 95% is achieved against the voltage fluctuation. From Fig. 4, the changing point between the half-bridge mode and the full-bridge mode is decided by the primary/the secondary side voltage including the turn ratio of the transformer.

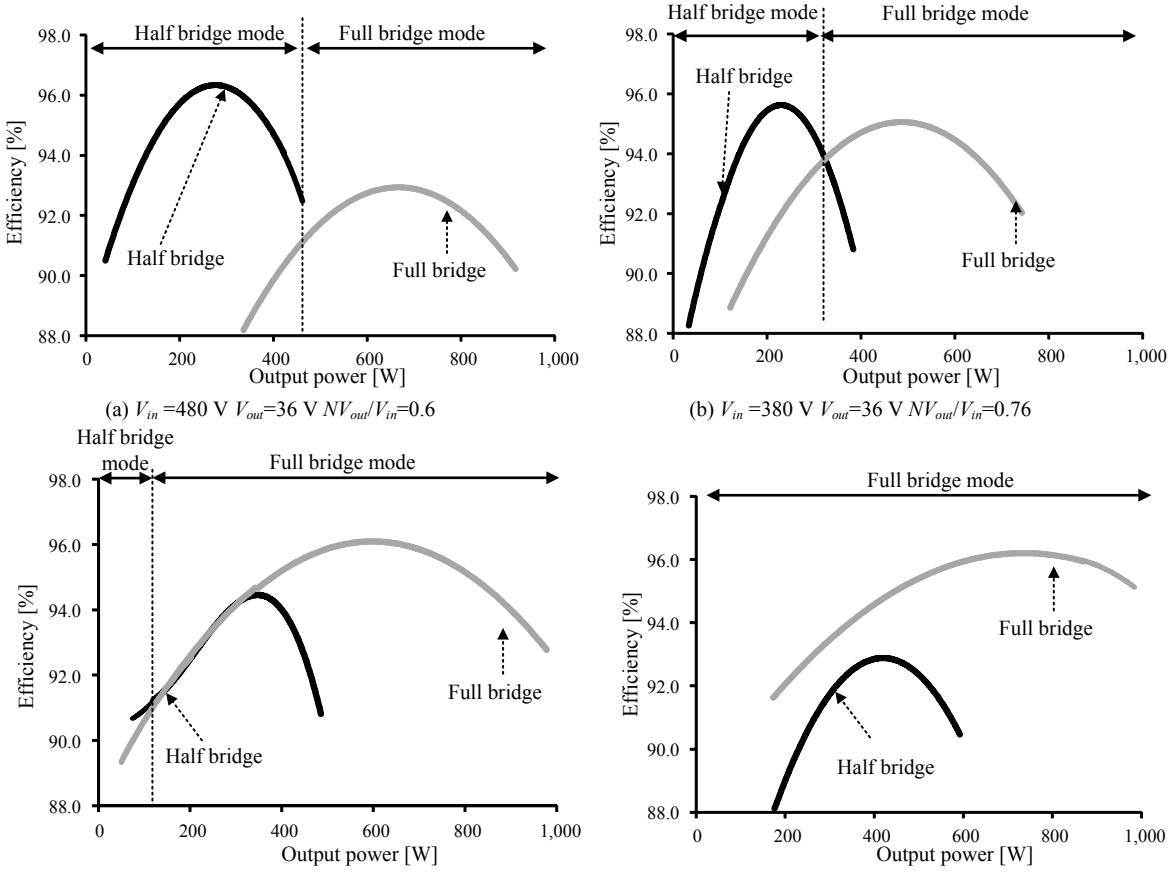

(a) V_{in} =480 V V_{out}=36 V NV_{out}/V_{in}=0.6

(b) V_{in} =380 V V_{out}=36 V NV_{out}/V_{in}=0.76

(c) V_{in} =380 V V_{out}=48 V NV_{out}/V_{in} =1

(d) V_{in} =380 V V_{out}=60 V NV_{out}/V_{in} =1.26

Fig. 4. Efficiency calculation results of proposed circuit.

Fig.4 (a) shows the efficiency against the output power when V_{in} is 480 V, V_{out} is 36 V. the efficiency of the half-bridge mode is much higher than the full-bridge mode at the light load. This is because the iron loss is decreased compared to the full bridge mode. However, the efficiency at the full-bridge mode is low. This is cause that the reactive current is large due to the error between the primary voltage and the secondary voltage including the turn ratio of the transformer. For the same reasons, the efficiency of the full-bridge mode becomes low at close to NV_{out}/V_{in}=0.5 (In Fig.4 (b) and (c)). On the other hand, In Fig. 4 (d), the efficiency of the full-bridge mode is increased when the ratio of the primary and the secondary inverter voltage including the turn ratio is close to 1.

Fig. 5 shows the changing point against NV_{out}/V_{in}. In order to derive the changing point against NV_{out}/V_{in}, equations (16) or (17), (1) is calculated using the specifications which are the input and the output voltage, the switching frequency, the leakage inductor and the turn ratio of the transformer. From Fig. 5, the good agreement with the simulation results. Moreover, the maximum error between the calculation and the simulation result is 4.3%. This is because the inductor current is varied by the dead-time. Therefore, the validity of changing point calculation is confirmed.

V. SIMULATION RESULTS

Fig. 6 shows the characteristics of the inductor current with three-level DAB converter and the two-level DAB converter. Fig. 6(a) shows the results when NV_{out}/V_{in} is set to 0.76. Fig. 6(b) shows the results when NV_{out}/V_{in}=0.5. At 33% load (300 W), the characteristic of the inductor current is sharply increased because the changing point between the full-bridge mode and the half-bridge mode at the 33% load (300 W). In Fig. 6(a), the inductor current is increased maximum 20% at 10% load (100 W). However, the iron loss is decreased by the half-bridge mode. In the loss calculation results, the efficiency is improved compared to the conventional DAB converter. Moreover, In Fig. 6(b), the inductor current is also reduced maximum 84% at 10% load (100 W) because the amplitude of the primary voltage is equal to the secondary voltage.

Fig. 7 shows the ZVS range against the inductor current between the three-level DAB converter and the two-level DAB converter. In Fig. 7, the ZVS is achieved at light load compared to the two-level DAB converter when the ratio of the input and the output voltage including the turn ratio of the transformer is $0.3>NV_{out}/V_{in}>1$. Especially, the output power for achievement of ZVS is from 5% load to 50% load in the case of NV_{out}/V_{in}=0.5 because the error between the ratio of the input/output voltage and the turn ratio of the transformer is zero. In addition, the ZVS range is extended by 60% compared to the two-level DAB converter. Therefore, the copper loss and the switching loss are reduced.

VI. EXPERIMENTAL RESULTS

In this section, the fundamental operation of the proposed DAB converter is verified by the prototype.

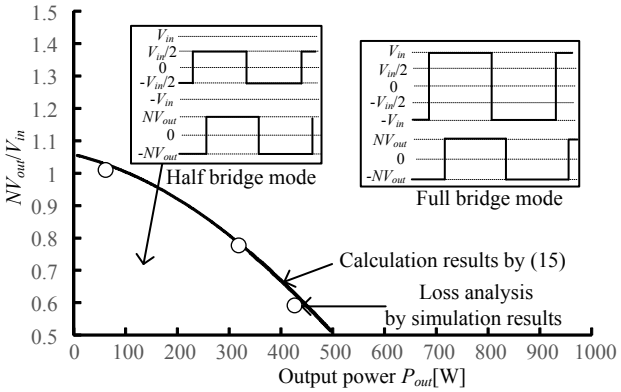

Fig. 5. Changing point between full-bridge mode and half-bridge mode by loss calculation.

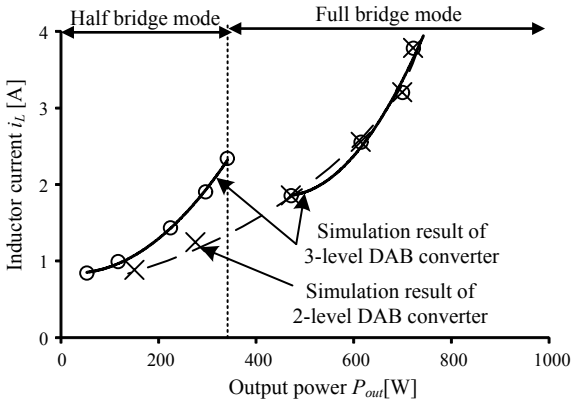

(a) NV_{out}/V_{in}=0.76

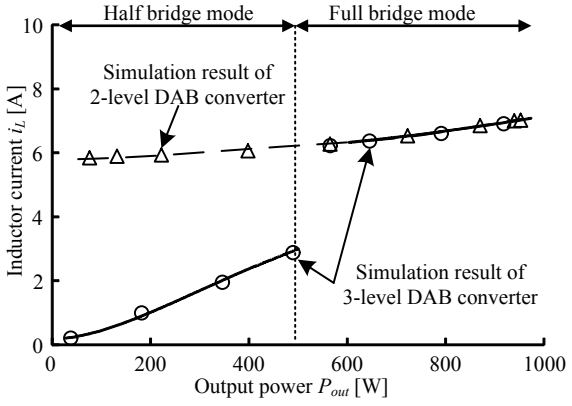

(b) NV_{out}/V_{in}=0.5

Fig. 6. Characteristic of the inductor current with three-level DAB converter and DAB converter

Fig. 8 shows the operation waveform of the proposed DC-DC converter. The input voltage V_{in} is 100 V. The output voltage V_{out} is 20 V. the switching frequency f_{sw} is 100 kHz. It is clear that the five-level waveform is output by the primary inverter. However, the output voltage of the primary inverter is not $1/2V_{in}$. This is because that the gate signals in the primary side switching devices are delayed by the gate drive circuit.

VII. CONCLUSTION

This paper proposed the DAB DC-DC converter utilizing to the three-level flying capacitor topology for the battery interface system. The operation mode of the three level DAB converter is determined by the loss calculation results. The theoretically with the maximum efficiency of over 95% in the full-bridge mode and the half-bridge mode. In addition, the validity of the changing point calculation is also confirmed. From the simulation results, the ZVS range is extended by 60%. In addition, the fundamental operation is validity.

In the future work, the operation mode including the five-level waveform will be derived using the loss calculation. Moreover, the validity of the proposed DAB converter is also confirmed by the experimental results.

REFERENCES

[1] Tatsuya Yamagishi, Hirofumi Akagi, Shin-ichi Kinouchi, Yuji Miyazaki, Masato Koyama: 「A 750-V,100-kW, 20-kHz Bidirectional Isolated DC/DC Converter Using SiC-MOSFET/SBD Modules」, IEEJ Trans. D, Vol. 134, No. 5, pp. 544-553 (2014)

[2] Tomohiro Matsuda, Giuseppe Guidi, Atsuo Kawamura Tomofumi Imakubo, Yuuji Imakubo, Yuuji Sasaki, Takehiro Jikumaru: 「Improvement of Efficiency of Dual Active Bridge DC-DC Converter by Using Pulse Width Modulation in AC Voltage」, JIASC2011, pp. 307-312 (2011)

[3] S. Inoue, H. Akagi: "A Bidirectional DC-DC Converter for an Energy Storage System With Galvanic Isolation", IEEE Trans on Power Electronics, Vol, 22, No. 6, pp. 2299-2306 (2007)

[4] Giuseppe Guidi, Atsuo Kawamura, Yuji Sasaki, Tomofumi Imakubo: 「Dual Active Bridge Modulation with Complete Zero Voltage Switching Taking Resonant Transitions into Account」, EPE2011, pp. 42014 (2011)

[5] Kheraluwala, M.N., Gascoigne, R.W., Divan, D.M., Baumann, E.D.: 「Preformance Characterization of a High Power Dual Active Bridge dc-to-dc Converter」, IEEE Trans. I.P., Vol. 28, No. 6, pp. 1294-1301 (1992)

[6] A. Jones, B. Smith, C. Maxwell: 「Reactive Power Loss Optimization Method for Bi-directional Isolated DC-DC Converters」, IEEE Trans. PE., Vol. 23, No. 6, pp. 2905-2914 (2008)

[7] Kheraluwala, M.N., Gascoigne, R.W., Divan, D.M., Baumann, E.D.: 「Preformance Characterization of a High Power Dual Active Bridge dc-to-dc Converter」, IEEE Trans. I.P., Vol. 28, No. 6, pp. 1294-1301 (1992)

[8] Rodriguez, J., Jih-Sheng Lai: 「Multilevel inverters; a survey of Topologies, Control, and Applications」, IEEE Trans. I.E., Vol. 49, No. 4, pp. 724-738 (2002)

[9] Moonem, M.A, Krishnaswami, H., Fang Zheng Peng: 「Control and Configuration of Three-Level Dual-Active Bridge Converter as a Front-end Interface for Photovoltaic System」, APEC2014, pp. 3017-3020 (2014)

[10] P. A. M. Bezerra, F. Krismer, R, M. Burkart, J. W. Kolar: 「Bidirectional Isolated Non-Resonant DAB DC–DC Converter for Ultra-Wide Input Voltage Range Applications」, PEAC2014, pp. 1038-1044 (201

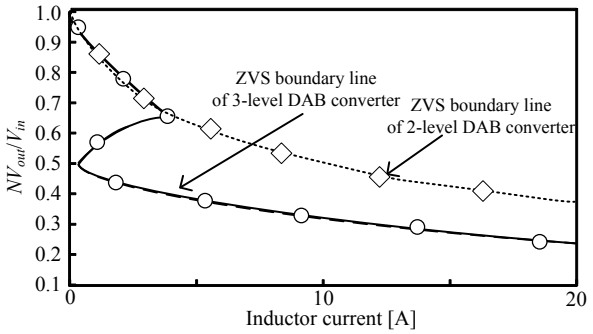

Fig. 7.Characteristic of ZVS range with three-level DAB converter and two-level DAB converter.

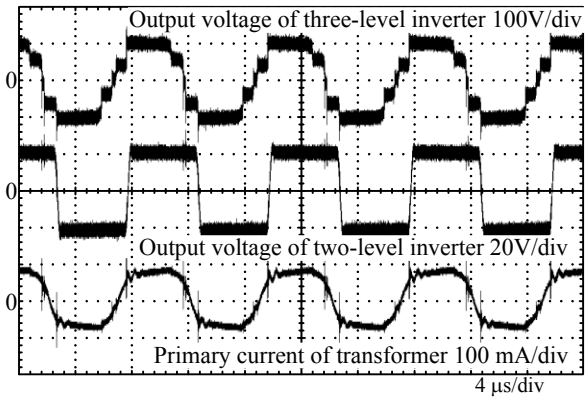

Fig. 8. Fundamental operation of proposed DAB converter.